Monthly Notices of the ROYAL ASTRONOMICAL SOCIETY

MNRAS **469,** 3840–3850 (2017) doi:10.1093/mnras/stx1144
Advance Access publication 2017 May 11

On the acceleration and deceleration of relativistic jets in active galactic nuclei – II. Mass loading

E. E. Nokhrina[1]★ and V. S. Beskin[1,2]

[1]*Moscow Institute of Physics and Technology, Institutsky per. 9, Dolgoprudny 141700, Russia*
[2]*Lebedev Physical Institute, Russian Academy of Sciences, Leninsky prospekt 53, Moscow 119991, Russia*

Accepted 2017 May 7. Received 2017 May 7; in original form 2016 November 16

ABSTRACT

The effect of mass loading of the magnetohydrodynamic (MHD) flow in relativistic jets from active galactic nuclei (AGNs) due to $\gamma\gamma \rightarrow e^+e^-$ conversion is considered analytically. We argue that the effects of charge average separation due to specific initial pairs' motion lead to partial magnetic and electric field screening or enhancement. The effect of the field screening has not been considered earlier. The pairs with the centre of mass moving faster or slower than the bulk plasma flow create a surface charge and a current that either screen or enhance both electric and magnetic fields in a pair creation domain. This impacts the bulk flow motion, which either accelerates or decelerates. The pairs with the centre of mass moving with exactly the drift velocity do not induce the field disturbance. In this case, the flow decelerates due to pure mass loading. For these different cases, the Lorentz factor of the loaded outflow is calculated as a function of loading pair number density. The effect may be important on sub-parsec to parsec scales due to the conversion of TeV jet radiation on the soft infrared to the ultraviolet external isotropic photon field. This leads to a jet outer shell acceleration. The conversion of MeV jet radiation on larger scales may account for the flow deceleration due to pure mass loading. The proposed mechanism may be a source of internal shocks and instabilities in the pair creation region.

Key words: radiation mechanisms: non-thermal – galaxies: active – galaxies: jets – quasars: general – radio continuum: galaxies.

1 INTRODUCTION

The recent Monitoring Of Jets in Active galactic nuclei with VLBA Experiments (MOJAVE) analysis of kinetic properties of the observed bright features of active galactic nuclei (AGNs) has shown that jets demonstrate predominantly negative acceleration of the order of $\dot{\Gamma}/\Gamma \sim 10^{-3}\text{to}10^{-2}$ yr^{-1} (Homan et al. 2015) at distances 20–100 pc from the jet cores. These are hard to explain within the ideal magnetohydrodynamical (MHD) models. On the other hand, on scales less than 10–20 pc the bright features tend to accelerate at the same rate. In Paper I (Beskin & Chernoglazov 2016), we have proposed that an accurate account for the drag force may explain the observed plasma deceleration, the characteristic length scales of deceleration being 100 pc. In this work, we put forward another possible mechanism for both jet acceleration and deceleration, i.e. the mass and charge loading due to two-photon pair creation.

The ideal MHD models of relativistic jets do not predict any radiation. The cold plasma moves with exactly the drift velocity in crossed electric and magnetic fields (Beskin 2009; Tchekhovskoy, McKinney & Narayan 2009), not undergoing any acceleration that may lead to radiation. Thus, in order to introduce the radiation site, one needs to create some particle energy disturbance – either by internal shocks or by means of instabilities. The proposed effect in this paper may account for such a site of radiation as well.

This paper follows a work where the radiation drag is considered self-consistently as a mechanism for plasma deceleration of a jet. Now we concentrate on charged pair loading. The mass loading itself has been considered by Lyutikov (2003) with the result of a flow acceleration as mass loading works effectively as a nozzle for the monopole magnetic field line geometry. The result does not depend on the charge of loaded particles in contrast with this paper. The work by Derishev et al. (2003) proposed a mechanism that may account for extremely efficient pair acceleration by switching the neutral–charged state of particles. The series of papers by Stern & Poutanen (2006, 2008) also explored the so-called photon breeding mechanism, in which the $\gamma\gamma$ pair conversion is followed by efficient acceleration of pairs and consequent high-energy radiation of photons (from where originates 'breeding'). These works are very close to what is done here since all of them also take advantage of charged particle behaviour in an electromagnetic field of a jet.

In this paper we consider the effects of charged pair loading on the relativistic jet dynamics. For the two-photon $\gamma\gamma \rightarrow e^+e^-$ pair conversion, we consider the dynamics of pairs in the ideal MHD bulk flow of cold jet plasma. In contrast with the latter, created pairs have relativistic temperature. Movement of a pair is determined

★E-mail: nokhrina@phystech.edu

by crossed electric and magnetic fields in a jet. If such pairs are created in some jet domain (e.g. an outer shell), the local electric and magnetic field screening takes place due to average charge separation and, consequently, appearance of electric and magnetic fields due to these charges and the corresponding currents. Locally, the drift velocity of plasma changes following the field screening, and this leads to either plasma acceleration due to the MHD process or plasma deceleration due to radiation of 'excess' energy.

In Section 3, we consider pairs created at rest in the laboratory frame (i.e. in the reference frame connected with the 'central engine'), thus moving backwards with respect to the jet bulk plasma outflow. We present the solution for such a case as being the most demonstrative and intuitively clear. For such simple initial conditions, we obtain the equation for the bulk Lorentz factor and the behaviour of flow magnetization after loading. Starting from microscopic motion, we calculate the energy-momentum tensor of loading pairs in Section 3.1. It is shown in Section 3.2 that the local screening of electric and magnetic fields is important and leads to bulk motion local deceleration and to the change in the integrals of motion as well. We estimate the appropriate change in a local magnetization of a flow in Section 3.3. In Section 4, the result of general initial conditions for pairs is obtained. We show that the pairs created in the centre-of-mass (c.m.) frame move faster than a jet that accelerates the bulk plasma due to electric and magnetic field enhancement. If the pairs are created with c.m. at rest in the jet proper frame, no field screening takes place, so the flow decelerates due to the pure mass loading. The luminosities in high-energy jet radiation are estimated to explain the acceleration and deceleration rates observed by Homan et al. (2015).

2 SETUP

In what follows, we will need a standard description of ideal axisymmetric MHD outflow. The magnetic field B and electric field E configuration is described by the magnetic flux function $\Psi(r,\varphi,z)$ in a cylindrical coordinate system with unit vectors $\{\boldsymbol{e}_r,\ \boldsymbol{e}_\varphi,\ \boldsymbol{e}_z\}$ by

$$\boldsymbol{B} = \frac{\nabla\Psi\times\boldsymbol{e}_\varphi}{2\pi r} - \frac{2I}{rc}\boldsymbol{e}_\varphi,$$

$$\boldsymbol{E} = -\frac{\Omega_\mathrm{F}}{2\pi c}\nabla\Psi, \tag{1}$$

where $\Omega_\mathrm{F}(\Psi)$ (Ferraro 1937) is an angular velocity and one of five integrals, i.e. functions preserved on the magnetic surfaces $\Psi=\mathrm{const}$ (see e.g. Beskin 2009 for more details). Here, c is the velocity of light. The other four are the entropy $s(\Psi)$, particle to magnetic flux ratio $\eta(\Psi)$, defined by

$$\boldsymbol{u} = \frac{\eta}{n}\boldsymbol{B} + \Gamma\frac{\Omega_\mathrm{F} r}{c}\boldsymbol{e}_\varphi, \tag{2}$$

and energy and momentum fluxes

$$E(\Psi) = \frac{\Omega_\mathrm{F} I}{2\pi c} + \mu\eta\Gamma,$$

$$L(\Psi) = \frac{I}{2\pi} + \mu\eta r u_\varphi. \tag{3}$$

Here the following physical properties of a flow are introduced: particle number density in a jet proper frame n (Beskin 2010), the total current I inside the magnetic tube, the flow bulk Lorenz factor Γ and the relativistic enthalpy μ. In what follows, we consider a cold flow $s=0$ so that $\mu = m_\mathrm{e}c^2$.

The important function that characterizes an MHD outflow is a magnetization, i.e. the ratio of the Poynting flux to the plasma kinetic energy flux:

$$\sigma = \frac{B^2}{4\pi m_\mathrm{e}c^2 n_\mathrm{lab}\Gamma}, \tag{4}$$

where n_lab is the particle number density in the laboratory frame, and it can be expressed through the particle number density in a jet proper frame n as $n_\mathrm{lab} = n\Gamma$. Using definition (1), the magnetization can be rewritten as

$$\sigma = \frac{\Omega_\mathrm{F} I}{2\pi m_\mathrm{e}c^3\eta\Gamma}. \tag{5}$$

3 PARTICLE LOADING – PAIRS CREATED AT REST

3.1 Particle motion

As already discussed in the introduction, the action of the pair loading on the magnetically dominated flow was mainly considered either phenomenologically (Derishev et al. 2003) or numerically (Stern & Poutanen 2006). Consistent analytical analysis for 1D (spherically symmetric) outflow was done by Lyutikov (2003). In particular, it was demonstrated that the action of particle loading is similar to negative pressure. On the other hand, shown below, some important properties (such as anisotropic pressure and redistribution of charges diminishing the electric and magnetic fields) were not taken into consideration. In the frame of the MHD approach briefly outlined in Section 2, the angular velocity Ω_F and the total current I change due to charge loading.

Following Lyutikov (2003), we consider here the simplest model of particle loading where the electron–positron pairs are created at rest in the nucleus rest frame (laboratory frame). This implies that these particles carry no energy E and angular momentum L flux, with the total gain in particle energy resulting from the diminishing of the Poynting flux of the magnetized wind.

Let us solve the equation of motion

$$\frac{\mathrm{d}u^i}{\mathrm{d}\tau} = \frac{e}{m_\mathrm{e}c}F^{ik}u_k, \tag{6}$$

for four-velocity of particle u^i with the initial condition in the nucleus rest frame $u^i(0)=\{1,0,0,0\}$. The solution is

$$\gamma(\tau) = \frac{B^2}{B'^2} - \frac{E^2}{B'^2}\cos\Omega'\tau, \tag{7}$$

$$u^r(\tau) = -\frac{E}{B'}\sin\Omega'\tau, \tag{8}$$

$$u^\varphi(\tau) = \frac{B_\mathrm{p}E}{B'^2}\left(1-\cos\Omega'\tau\right), \tag{9}$$

$$u^z(\tau) = \frac{B_\varphi E}{B'^2}\left(1-\cos\Omega'\tau\right). \tag{10}$$

Here, B and E are the magnetic and electric fields in the laboratory frame, $B' = \sqrt{B^2-E^2}$ is a field in a jet frame, τ is the proper time in the charges comoving frame (which is different from the jet proper frame) and

$$\Omega' = \frac{eB'}{m_\mathrm{e}c} \tag{11}$$

is a proper gyrofrequency, i.e. gyrofrequency in a jet proper frame instantly coincident with plasma bulk motion, which is essentially a drift motion in crossed magnetic and electric fields.

Assuming the pairs are created uniformly over the jet, we average the velocities and energy at a given space point over all the particles with trajectories crossing this point. This is equivalent to averaging over the gyroperiod, with the procedure details described in Appendix A. So, we obtain the following Lorentz factor and velocities:

$$\langle\gamma\rangle = \Gamma^2\left(1+\frac{\beta^4}{2}\right), \tag{12}$$

$$\langle v_r\rangle = 0, \tag{13}$$

$$\langle v_z\rangle = c\beta\cos\alpha, \tag{14}$$

$$\langle v_\varphi\rangle = c\beta\sin\alpha. \tag{15}$$

Here we use the relation $B^2/B'^2 = \Gamma^2$ with Γ being the Lorentz factor of the drift velocity, $\beta = \sqrt{1-\Gamma^{-2}}$ is the drift velocity, $\cos\alpha = B_\varphi/B$ and $\sin\alpha = B_\mathrm{p}/B$.

We stress that the mean energy of the individual loaded particle ϵ_ld exceeds essentially the energy of particles in a jet $\epsilon_\mathrm{jet} = m_\mathrm{e}c^2\Gamma$:

$$\epsilon_\mathrm{ld} = m_\mathrm{e}c^2\langle\gamma\rangle \approx \frac{3}{2}m_\mathrm{e}c^2\Gamma^2. \tag{16}$$

However, the mean velocity of each loaded particle coincides with the drift velocity of plasma in a jet:

$$\langle\boldsymbol{v}_\mathrm{ld}\rangle = \boldsymbol{v}_\mathrm{drift}. \tag{17}$$

This implies that loading supplies the initially cold plasma with relativistic particles.

Let us determine the thermodynamical parameters calculating the components of the energy-momentum tensor T^{ik}_ld of loaded particles. In order to do it, we average the components of the tensor

$$T^{ik}_\mathrm{ld} = m_\mathrm{e}c^2\langle n^\mathrm{rest}u^i u^k\rangle \tag{18}$$

(see Appendix B for more details) and compare the result with the form of energy-momentum tensor expressed through the internal energy density ε_ld, longitudinal P_n and transverse P_s components of the pressure with respect to the magnetic field (Tsikarishvili, Rogava & Tsikauri 1995; Kuznetsova 2005) and hydrodynamical four-velocity U^i:

$$T^{ik}_\mathrm{ld} = \left(\varepsilon_\mathrm{ld}+P_\mathrm{s}+\frac{\boldsymbol{b}^2}{4\pi}\right)U^iU^k + \left(P_\mathrm{s}+\frac{\boldsymbol{b}^2}{8\pi}\right)g^{ik} - \left(\frac{P_\mathrm{s}-P_\mathrm{n}}{\boldsymbol{b}^2}+\frac{1}{4\pi}\right)b^ib^k. \tag{19}$$

Here $\mathbf{b}^2$ is the plasma proper magnetic field energy density, and

$$b^i = \frac{1}{2}\eta^{ijkl}U_jF_{kl} \tag{20}$$

is the Lichnerowicz (Lichnerowicz 1967; Asséo & Beaufils 1983) four-vector ($b^2 = B'^2$). It gives for the internal energy density of loaded particles

$$\varepsilon_\mathrm{ld} = m_\mathrm{e}c^2n_\mathrm{ld}\Gamma \tag{21}$$

and for pressure components

$$P_\mathrm{n} = 0, \tag{22}$$

$$P_\mathrm{s} = \frac{1}{2}m_\mathrm{e}c^2n_\mathrm{ld}\beta^2\Gamma. \tag{23}$$

Hence, the energy-momentum tensor (19) corresponds to anisotropic pressure with $P_\mathrm{n} = 0$ resulting from particle rotation in the rz-plane only. Thus, at this point our approach differs from the one considered by Lyutikov (2003). It is important that in the cylindrical geometry under consideration the volume force $\mathcal{F}_i = -\nabla_k P_{ik}$ appears even for a constant value P_s:

$$\mathcal{F} = -\frac{P_\mathrm{s}}{r}\boldsymbol{e}_r. \tag{24}$$

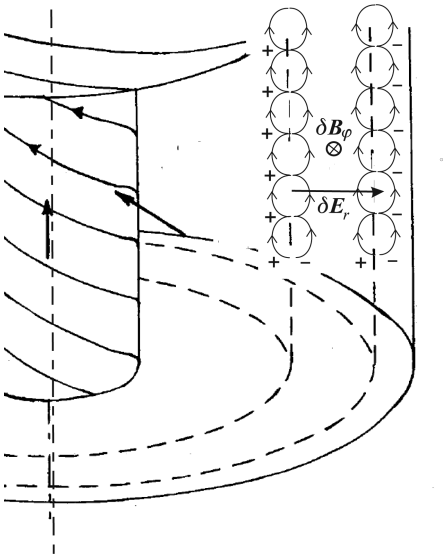

Figure 1. Cartoon of the loading plasma trajectories and induced electric and magnetic fields.

3.2 Mass-loaded flow properties

The problem of pair loading the MHD flow is its impact on the angular velocity Ω_F, which describes the electric field, and the current I, which describes the toroidal component of the magnetic field. We argue that both quantities change due to charge loading, and its effect on the jet dynamics is significant and cannot be reduced to pure redistribution of energy between the cold plasma with unchanged Ω_F and I and loaded plasma.

Indeed, pairs initially created at rest start cycloid movement in crossed electric and magnetic fields with the radial velocity component directed oppositely for electrons and positrons (it is obvious when one notices that the charge sign appears in gyrofrequency Ω'). This leads to mean over gyroperiod separation (see Fig. 1) of positive and negative charges in the r direction:

$$r_\perp = \langle r^+(\tau) - r^-(\tau)\rangle = -\frac{m_\mathrm{e}c^2\beta\Gamma^2}{eB}\left(2+\beta^2\right). \tag{25}$$

In the simplest case of a shell domain with the uniform loaded particle number density n_ld as measured in a jet proper frame, the sides of a constant r possess a surface charge σ_e and a surface current $\sigma_\mathrm{e}v_\mathrm{drift}$. Indeed, if pairs are created uniformly over a shell $\{L_\mathrm{r}, r\Delta\varphi, L_\mathrm{z}\}$ with mean separation $r_\perp$ in the r direction, this can be envisioned as two shells with uniformly distributed positive and negative charges, shifted in the r direction on the mean charge separation $r_\perp$. The total charges on opposite faces are $\pm enr_\perp r\Delta\varphi L_z$, with effective surface charge density being $\sigma_\mathrm{e} = enr_\perp$. As pairs are moving in crossed electric and magnetic fields with the drift velocity, there is a surface current of opposite signs flowing along the r boundaries of a pair creation domain. The significant magnetic field due to these currents is inside this domain. These charge and current densities partially screen the initial electric and magnetic fields. This must lead to a change in the bulk jet velocity, depending on the proportion in which fields were screened.

The effect of jet acceleration or deceleration in this model may be obtained self-consistently. We designate all the flow characteristics after mass loading by tilde. They are the screened electric and magnetic fields, the appropriate Lorentz factor of a jet bulk motion and so forth. We assume that the proper motion of loaded particles is determined by these screened fields. In particular, we substitute the parameters of accelerated flow and the screened fields into the expression for the average charge separation (25). Thus, in equation (25) we use the fluid velocity $c\tilde{\beta}$, Lorentz factor $\tilde{\Gamma}$ and screened magnetic field $\tilde{B}$ instead of initial unperturbed flow parameters.

The surface charge in a laboratory frame is equal to

$$\sigma_{\rm e} = en_{\rm ld}^{\rm lab} r_{\perp} = e\tilde{\Gamma} n_{\rm ld} r_{\perp}, \tag{26}$$

where $r_{\perp}$ is a mean over laboratory time (or, equally, over the loaded particle ensemble) charge separation. The associated electric field disturbance for the given loaded particle number density is

$$\delta E = \frac{4\pi m_{\rm e} c^2 n_{\rm ld} \tilde{\beta}^2 \tilde{\Gamma}^3}{\tilde{E}} \left(2 + \tilde{\beta}^2\right). \tag{27}$$

The appropriate magnetic field disturbance δB produced by two opposite surface currents flowing along the domain boundaries of a constant r is $\delta B = \tilde{\beta}\delta E$, which gives

$$\delta B = \frac{4\pi m_{\rm e} c^2 n_{\rm ld} \tilde{\beta}^2 \tilde{\Gamma}^3}{\tilde{B}} \left(2 + \tilde{\beta}^2\right). \tag{28}$$

The fields are disturbed only locally in the mass loading domain. The proposed self-similar way of calculating the electric and magnetic fields is applicable while the disturbance is much less than the initial fields. So, we imply that $\delta B/B \ll 1$ or equally

$$\frac{1}{\sigma}\frac{n_{\rm ld}}{n}\Gamma\beta^2\left(1 + \frac{\beta^2}{3}\right) \ll 1. \tag{29}$$

Here, let us note that such a screening will indeed lead to a jet deceleration. The initial fields correlate as $E = \beta B$. The fields created by loaded particles correlate as $\delta B = \tilde{\beta}\delta E$, so the magnetic field screening is less than that of the electric field. This leads to a smaller drift velocity $\tilde{\beta} = (E - \delta E)/(B - \delta B)$.

Let us obtain the local (in a pair creation domain) self-consistent drift velocity $\tilde{\beta}$ of bulk plasma due to field screening. The fields now depend on $\tilde{\Gamma}$ and $n_{\rm ld}$:

$$\tilde{B} = \frac{B}{2}\left[1 + \sqrt{1 - \frac{4}{\sigma}\frac{n_{\rm ld}}{n}\frac{\tilde{\Gamma}^3}{\Gamma^2}\tilde{\beta}^2\left(2 + \tilde{\beta}^2\right)}\right], \tag{30}$$

$$\tilde{E} = \frac{E}{2}\left[1 + \sqrt{1 - \frac{4}{\sigma}\frac{n_{\rm ld}}{n}\frac{\tilde{\Gamma}^3}{\Gamma^2}\frac{\tilde{\beta}^2}{\beta^2}\left(2 + \tilde{\beta}^2\right)}\right]. \tag{31}$$

Here, we use the expression for a flow magnetization given by (4).

The explicit equation on $\tilde{\Gamma}$ is

$$\tilde{\Gamma} = \frac{\tilde{B}}{\sqrt{\tilde{B}^2 - \tilde{E}^2}}, \tag{32}$$

where $\tilde{B} = B - \delta B$ and $\tilde{E} = E - \delta E$, which,through (30)–(31), depend themselves on $\tilde{\Gamma}$ and $n_{\rm ld}$. After some tiresome algebra, one can obtain the following algebraic equation on $\tilde{\Gamma}$:

$$\begin{aligned}
&-16\tilde{\Gamma}^{10} - 24\tilde{\Gamma}^9 q\left(2\Gamma^2 - 1\right) + \tilde{\Gamma}^8\left[32 - 9q^2\right] \\
&+ 56\tilde{\Gamma}^7 q\left(2\Gamma^2 - 1\right) + \tilde{\Gamma}^6\left[16\left(\Gamma^4 - \Gamma^2 - 1\right) + 24q^2\right] \\
&- 40\tilde{\Gamma}^5 q\left(2\Gamma^2 - 1\right) + \tilde{\Gamma}^4\left[-16\left(\Gamma^4 - \Gamma^2\right) - 22q^2\right] \\
&+ 8\tilde{\Gamma}^3 q\left(2\Gamma^2 - 1\right) + 4\tilde{\Gamma}^2 q^2 - q^2 = 0,
\end{aligned} \tag{33}$$

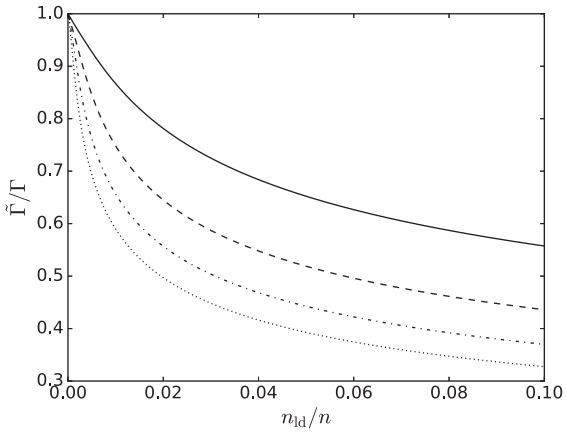

Figure 2. Relative Lorentz factor $\tilde{\Gamma}/\Gamma$ is plotted as a function of the relative loading particle number density $n_{\rm ld}/n$ for different initial Γ. The solid curve corresponds to $\Gamma = 5$, dashed to $\Gamma = 10$, dash–dotted to $\Gamma = 15$ and dotted to $\Gamma = 20$.

where

$$q = \frac{4}{\sigma}\frac{n_{\rm ld}}{n}. \tag{34}$$

We see in Fig. 2 that for a fairly moderate ratio $n_{\rm ld}/n$ the jet deceleration effect is appreciable. The effect is more pronounced for the faster jets.

3.3 Loaded flow magnetization

Now we are ready to discuss back reaction of the particle loading on the properties of the magnetically dominated flow. We suppose that the magnetized jet consists of electromagnetic field, cold particle flow (number density in the comoving reference frame n and relativistic enthalpy μ) and loading particles with the energy-momentum tensor $T_{\rm ld}^{ik}$ (19), both components having the same hydrodynamical velocity $\langle \boldsymbol{v} \rangle$.

General expressions for the energy $E(\Psi)$ and angular momentum $L(\Psi)$ fluxes of the ideal relativistic MHD flow with anisotropic pressure (Asséo & Beaufils 1983; Tsikarishvili et al. 1995; Kuznetsova 2005) include a standard anisotropic pressure parameter

$$\beta_{\rm a} = 4\pi\frac{P_{\rm n} - P_{\rm s}}{b^2}. \tag{35}$$

In our case, $\beta_{\rm a} < 0$. For steady-state flow, the energy conservation is written as

$$\mathrm{div}\ \boldsymbol{S} = 0, \tag{36}$$

where $S^i = T^{0i}$. In the case of a cylindrical axisymmetric flow for the given Lichnerowicz (1967) vector (see Appendix B) with $b^0 = 0$, it transforms into

$$\frac{\partial}{\partial z}\left(\frac{\boldsymbol{b}^2}{4\pi} + P_{\rm s} + \varepsilon_{\rm ld} + \varepsilon_{\rm bulk}\right)\tilde{\Gamma}^2\tilde{v}_z = 0, \tag{37}$$

and after integration over z we obtain

$$E(\Psi)B_{\rm p} = \mathrm{const}, \tag{38}$$

with the energy flux

$$E(\Psi) = \frac{\tilde{\Omega}_{\rm F}\tilde{I}}{2\pi c}(1 + |\beta_{\rm a}|) + \mu_{\rm ld}\eta_{\rm ld}\tilde{\Gamma} + \mu\eta\tilde{\Gamma}. \tag{39}$$

Each of the four terms in (39) originates from the appropriate term in (37). The angular momentum flux is

$$L(\Psi) = \frac{\tilde{I}}{2\pi}(1 + |\beta_{\rm a}|) + \mu_{\rm ld}\eta_{\rm ld} r_\perp \tilde{u}_\varphi + \mu\eta r_\perp \tilde{u}_\varphi. \tag{40}$$

Expressions (39) and (40) are sums of standard relations for cold flow (3) and appropriate terms for loaded charged pairs. We must note here that the angular velocity $\tilde{\Omega}_{\rm F}$ and the current density $\tilde{I}$ are defined by the screened electric and magnetic fields. Here particle-to-magnetic flux ratios for initial $\eta(\Psi)$ and loading $\eta_{\rm ld}(\Psi)$ plasma are determined by the standard relations

$$\begin{aligned} \boldsymbol{u} &= \frac{\eta}{n}\tilde{\boldsymbol{B}} + \tilde{\Omega}_{\rm F} r_\perp \tilde{\Gamma}\boldsymbol{e}_\varphi, \\ \boldsymbol{u}_{\rm ld} &= \frac{\eta_{\rm ld}}{n_{\rm ld}}\tilde{\boldsymbol{B}} + \tilde{\Omega}_{\rm F} r_\perp \tilde{\Gamma}\boldsymbol{e}_\varphi. \end{aligned} \tag{41}$$

Since $\langle \boldsymbol{u}_{\rm ld}\rangle = \boldsymbol{u}$ one can conclude that $\eta_{\rm ld} = \eta n_{\rm ld}/n$. Finally, $\mu = \varepsilon/n = mc^2$ and $\mu_{\rm ld} = \varepsilon_{\rm ld}/n_{\rm ld} = mc^2\tilde{\Gamma}$. In (39) and (40), the first terms $\tilde{\Omega}_{\rm F}\tilde{I}/2\pi c$ and $\tilde{I}/2\pi$ correspond to the electromagnetic flux, while the second and third ones describe the fluxes corresponding to anisotropic pressure and internal energy of the loading particles, respectively. The last terms correspond to cold wind.

Taking into account the results of Section 3.2, we can find a loaded flow magnetization. As secondary particles in the simple problem stated in Section 3.1 carry zero energy flux (39), we may equate the corresponding integrals E before and after loading:

$$\frac{\Omega_{\rm F} I}{2\pi c} + \mu\eta\Gamma = \frac{\tilde{\Omega}_{\rm F}\tilde{I}}{2\pi c}(1 + |\beta_{\rm a}|) + \mu_{\rm ld}\eta_{\rm ld}\tilde{\Gamma} + \mu\eta\tilde{\Gamma}. \tag{42}$$

This expression allows us to calculate the magnetization of the mass-loaded flow. Indeed, one can rewrite the Poynting flux using standard functions $\tilde{\Omega}_{\rm F}$ and $\tilde{I}$ as

$$\tilde{\boldsymbol{S}} = \frac{1}{2\pi c}\tilde{\Omega}_{\rm F}\tilde{I}\tilde{\boldsymbol{B}}_{\rm p}. \tag{43}$$

This corresponds to the first term on the RHS in the energy flux (42). The other three terms are anisotropic pressure of loaded flow, motion of loaded relativistic plasma and bulk motion of jet plasma. We must stress that the term with parameter $|\beta_{\rm a}|$, although being traditionally written using the Poynting flux, is related to the plasma internal energy, carried by loaded particles (see equation 37). Thus, the definition of the magnetization parameter after loading is

$$\tilde{\sigma} = \left(\frac{\tilde{\Omega}_{\rm F}\tilde{I}}{2\pi c}\right)\left(\frac{\tilde{\Omega}_{\rm F}\tilde{I}}{2\pi c}|\beta_{\rm a}| + \mu_{\rm ld}\eta_{\rm ld}\tilde{\Gamma} + \mu\eta\tilde{\Gamma}\right)^{-1}. \tag{44}$$

Using (42), we finally obtain the relation for the magnetization of loaded flow as

$$\tilde{\sigma} = \sigma\left(\frac{\tilde{S}}{S}\right)\left[\frac{\tilde{\Gamma}}{\Gamma}\left(1 + \tilde{\Gamma}\frac{n_{\rm ld}}{n}\right) + \frac{n_{\rm ld}}{n}\frac{\tilde{\Gamma}^3}{\Gamma^2}\frac{\tilde{\beta}^3}{2\beta}\right]^{-1}. \tag{45}$$

We plot in Fig. 3 the loaded magnetization $\tilde{\sigma}$ as a function of the loading particle number density $n_{\rm ld}$ for different initial bulk flow Lorentz factors Γ. As one can see, for $\Gamma = 5$ and 10 the magnetization drops. However, for greater Lorentz factors it grows and becomes more than unity. It has been noted in Section 3.2 that the charge loading screens the electric field greater than the magnetic field. As a consequence, the Poynting flux of a flow always drops. But the initial faster flow decelerates more effectively, so for greater Lorentz factors the drop in the kinetic energy flux is greater than that in the Poynting flux, which leads to the growth of the flow magnetization. For $n_{\rm ld}/n \to +0$, the magnetization always decreases as

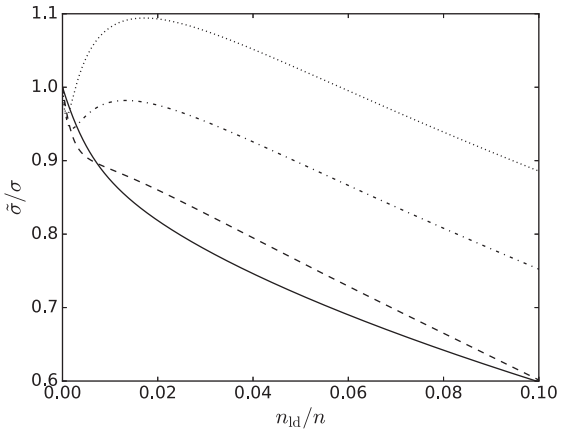

Figure 3. Relative magnetization $\tilde{\sigma}/\sigma$ is plotted as a function of the relative loading particle number density $n_{\rm ld}/n$ for different initial Γ. The solid curve corresponds to $\Gamma = 5$, dashed to $\Gamma = 10$, dash–dotted to $\Gamma = 15$ and dotted to $\Gamma = 20$.

$$\frac{\tilde{\sigma}}{\sigma} = 1 - \left(\frac{3}{2} + \frac{3}{\sigma}\right)\frac{n_{\rm ld}}{n}\Gamma \approx 1 - \frac{9}{2}\frac{n_{\rm ld}}{n}\Gamma, \tag{46}$$

which can be seen in Fig. 3. This implies that for a small enough loading particle number density the field screening, and so the diminishing of the Poynting flux, is more important than the flow deceleration itself.

We must stress again that the screening of electric and magnetic fields is important for arbitrarily low pair loading. Indeed, suppose that $q \to +0$, so $\tilde{\Gamma} \to \Gamma - 0$. In this case, we can retain the leading terms in equation (33):

$$16\tilde{\Gamma}^6\Gamma^4 - 16\tilde{\Gamma}^{10} - 48q\tilde{\Gamma}^9\Gamma^2 = 0 \tag{47}$$

and obtain

$$\tilde{\Gamma} = \Gamma - \frac{3}{\sigma}\frac{n_{\rm ld}}{n}\Gamma^2. \tag{48}$$

This relation corresponds to a tangent line to any curve in Fig. 2 at $n_{\rm ld}/n = 0$.

On the other hand, we may propose that for extremely low loaded particle number density the effects of the electric and magnetic field screening is negligible, and the angular velocity $\Omega_{\rm F}$ and current I do not change. Under this assumption one can obtain from (42)

$$\Gamma - \tilde{\Gamma} = \frac{3}{2\sigma}\frac{n_{\rm ld}}{n}\Gamma^2, \tag{49}$$

which is in contradiction with (48). This implies that the effect of screening of the electric and magnetic fields is important for any rate of pair loading, and, apparently, it has not been taken into consideration by the previous works. When the loading particle number density tends to zero, the deceleration rate is greatest and can be expressed in the following short form:

$$\frac{\dot{\Gamma}}{\Gamma} = -\frac{3\Gamma}{2\sigma}\frac{\dot{n}}{n}. \tag{50}$$

4 EFFECTS OF PAIRS CREATED WITH ARBITRARY VELOCITIES

In Section 3, we have considered pairs created at rest in the laboratory frame. Let us now consider the effects of particle loading if

pairs are created with their c.m. moving with the velocity β_0 and corresponding Lorentz factor Γ_0 along the jet. If the energies of interacting photons are greater than threshold, electron and positron are created with Lorentz factors γ_0' and isotropically distributed velocities β_0' in the c.m. frame. The direction of velocity for electron/positron in the c.m. frame is set by spherical angles θ' and φ'. The initial conditions for such a pair are

$$\begin{aligned}
\gamma_{0\pm} &= \Gamma_0\gamma_0'\left(1 \pm \beta_0\beta_0'\cos\theta'\right),\\
u^r_{0\pm} &= \mp\gamma_0'\beta_0'\sin\theta'\cos\varphi',\\
u^z_{0\pm} &= \Gamma_0\gamma_0'\left(\beta_0 \pm \beta_0'\cos\theta'\right).
\end{aligned} \tag{51}$$

Here, plus and minus designate the positive and negative charges, as the initial conditions at the laboratory frame are different for them. The particle Lorentz factor and r-component of four-velocity are

$$\begin{aligned}
\gamma_\pm(\tau) &= \Gamma^2\left(\gamma_{0\pm} - \beta u^z_{0\pm}\right)\\
&\quad + \cos\Omega'\tau\Gamma^2\beta\left(u^z_{0\pm} - \beta\gamma_{0\pm}\right)\\
&\quad \pm \sin\Omega'\tau\beta\Gamma u^r_{0\pm},\\
u^r_\pm(\tau) &= \cos\Omega'\tau u^r_{0\pm} \pm \sin\Omega'\tau\Gamma\left(u^z_{0\pm} - \beta\gamma_{0\pm}\right).
\end{aligned} \tag{52}$$

The r-coordinate for each charge is

$$\begin{aligned}
r_\pm(\tau) &= \left[R_0 \pm \frac{c\Gamma}{\Omega'}\left(u^z_{0\pm} - \beta\gamma_{0\pm}\right)\right]\\
&\quad \mp \cos\Omega'\tau\frac{c\Gamma}{\Omega'}\left(u^z_{0\pm} - \beta\gamma_{0\pm}\right) + \sin\Omega'\tau\frac{c}{\Omega'}u^r_{0\pm}.
\end{aligned} \tag{53}$$

In order to obtain the mean charge displacement, we need to average the particle displacement at every space point over the particle ensemble. The direction of initial velocity of each charge in the c.m. frame is isotropic. The trajectory phase $\varphi = \Omega'\tau$ has a weight function $\gamma_\pm(\tau)$ since each charge spends different laboratory times on each part of its gyration trajectory. Thus, the full distribution function is

$$f_\pm(\theta',\,\varphi',\,\varphi) = \gamma_\pm(\theta',\,\varphi',\,\varphi), \tag{54}$$

with the normalization included explicitly.

Obviously, for a given pair the Lorentz factors of electron and positron are different, so we define the average charge displacement as

$$\begin{aligned}
r_\perp &= \langle r_+\rangle - \langle r_-\rangle\\
&= \int r_+ f_+ \mathrm{d}\Omega_{\theta'\varphi'}\mathrm{d}\tau\left(\int f_+\mathrm{d}\Omega_{\theta'\varphi'}\mathrm{d}\tau\right)^{-1}\\
&\quad - \int r_- f_-\mathrm{d}\Omega_{\theta'\varphi'}\mathrm{d}\tau\left(\int f_-\mathrm{d}\Omega_{\theta'\varphi'}\mathrm{d}\tau\right)^{-1}.
\end{aligned} \tag{55}$$

Using this expression, one can find the mean charge displacement

$$\begin{aligned}
r_\perp &= \frac{m_\mathrm{e}c^2\tilde\Gamma^2}{e\tilde B}\Gamma_0\gamma_0'\left[2(\beta_0 - \tilde\beta)\left(1 + \frac{\beta_0'^2}{3}\right)\right.\\
&\quad \left. - \tilde\beta\frac{\left(\beta_0 - \tilde\beta\right)^2}{1 - \tilde\beta\beta_0} - \tilde\beta(1 - \tilde\beta\beta_0)\frac{\beta_0'^2}{3}\right].
\end{aligned} \tag{56}$$

Three different limits can be considered for the problem.

4.1 Deceleration along the jet due to field screening

The first case corresponds to condition $\Gamma_0 \ll \Gamma$. As the limiting case we set $\Gamma_0 = 1$ which leads to

$$r_\perp = -\frac{m_\mathrm{e}c^2\tilde\beta\tilde\Gamma^2}{e\tilde B}\gamma_0'\left(2 + \tilde\beta^2 + \beta_0'^2\right). \tag{57}$$

This is exactly the loading considered in the previous section, but for the loaded particles with higher initial temperature. Thus, the effect of the field screening is even more pronounced for non-zero β_0'. Indeed, we see from equations (25) and (57) that the average charge displacements $r_\perp$ differ by the factor

$$f_1 = \frac{\gamma_0'\left(2 + \tilde\beta^2 + \beta_0'^2\right)}{2 + \tilde\beta^2} \geq 1. \tag{58}$$

Thus, all the results of Section 3.2 are applicable if we divide the loading particle number density by f_1. In particular, we need to load the flow by f_1-times less charge number density than in Section 3.2 in order to achieve the same deceleration rate. However, as the reaction cross-section behaves as $\sigma_{\gamma\gamma} \propto (\ln 2x - 1)/x^2$, where x is a photon energy normalized on the electron rest mass in the c.m. system (see e.g. Svensson 1982), the pairs are more likely created with non-relativistic or mildly relativistic speeds with respect to the c.m. system.

We must note that although the impact of charges creation described in Sections 3 and 4.1 with c.m. moving slower than the jet initial bulk velocity is very illustrative, the physical conditions that lead to such a pair creation can hardly be imagined in the jet environment. So, we proceed to the cases that have astrophysical applications.

4.2 Pure mass loading

The condition $\Gamma_0 \approx \Gamma$ and $\beta_0 \approx \beta$ corresponds to the case when c.m. of each pair is moving with the hydrodynamic velocity. As can be seen from the general expression for the average charge displacement (56), no charge separation and, consequently, no field screening take place in this case. The effect of flow deceleration is purely due to mass loading.

However, due to cylindrical jet geometry this will lead not to the flow acceleration, but to a flow deceleration. Pairs created in a c.m. reference frame at rest with reference to bulk flow motion do not contribute to electric and magnetic field screening/enhancement. Thus, there is no change in the integral $\Omega_\mathrm{F}(\Psi)$, corresponding to the electric field, and in the total current I, corresponding to the magnetic field. The analysis of the effect of deceleration is even simpler in this case, and the deceleration rate can be obtained through the examination of the expression for the integral $E(\Psi)$ solely.

Using the known charge motion (51) and (52) with $\Gamma_0 = \Gamma$ and $\beta_0 = \beta$, we obtain

$$\begin{aligned}
T^{00}_\mathrm{ld} &= m_\mathrm{e}c^2 n_\mathrm{ld}\Gamma^2\gamma_0'\left(1 + \beta^2\frac{\beta_0'^2}{3}\right),\\
T^{11}_\mathrm{ld} &= m_\mathrm{e}c^2 n_\mathrm{ld}\gamma_0'\frac{\beta_0'^2}{3}.
\end{aligned} \tag{59}$$

From these we get the internal energy density and pressure

$$\begin{aligned}
\varepsilon_\mathrm{ld} &= m_\mathrm{e}c^2 n_\mathrm{ld}\gamma_0',\\
P_\mathrm{s} &= m_\mathrm{e}c^2 n_\mathrm{ld}\gamma_0'\frac{\beta_0'^2}{3}.
\end{aligned} \tag{60}$$

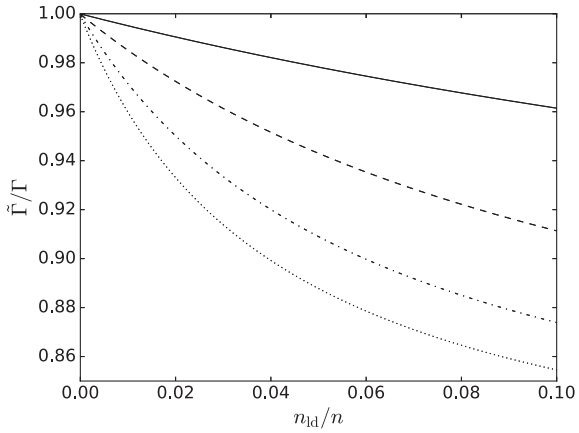

Figure 4. The deceleration due to pure mass loading. Ratio of the Lorentz factors after and before loading is plotted as a function of the relative loading particle number density $n_{\rm ld}/n$ for different γ_0'. The solid curve corresponds to $\gamma_0' = 2$, dashed to $\gamma_0' = 5$, dash–dotted to $\gamma_0' = 10$ and dotted to $\gamma_0' = 15$.

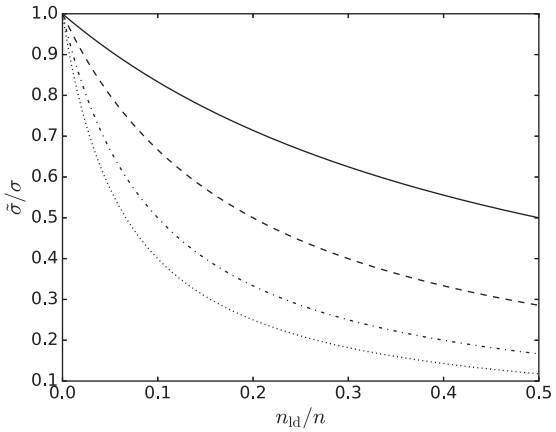

Figure 5. The deceleration due to pure mass loading. Ratio of the flow magnetization after and before loading is plotted as a function of the relative loading particle number density $n_{\rm ld}/n$ for different γ_0'. The solid curve corresponds to $\gamma_0' = 2$, dashed to $\gamma_0' = 5$, dash–dotted to $\gamma_0' = 10$ and dotted to $\gamma_0' = 15$.

The particle energy flux before mass loading is defined by equation (3) and after mass loading by equation (39). But the total change in the energy flux is equal to the energy flux of created pairs,

$$\Delta E = m_{\rm e}c^2\eta\gamma_0'\frac{n_{\rm ld}}{n}\Gamma. \tag{61}$$

Thus, we equate the energy fluxes before and after loading:

$$\frac{\Omega_{\rm F}I}{2\pi c} + \mu\eta\Gamma + \Delta E = \frac{\Omega_{\rm F}I}{2\pi c}\left(1 + \frac{4\pi\tilde{\Gamma}^2}{B^2}P_{\rm s}\right) + \mu\eta\tilde{\Gamma} + \mu\eta\gamma_0'\frac{n_{\rm ld}}{n}\tilde{\Gamma}. \tag{62}$$

Obviously, for $\beta_0' = 0$ there is no change in the flow Lorentz factor because the cold plasma loaded with the average drift velocity does not contribute to the change in the bulk flow velocity. For relativistic plasma, we obtain the following relation on $\tilde{\Gamma}$ of decelerated flow for given β_0' and $n_{\rm ld}$:

$$\frac{\tilde{\Gamma}^2}{\Gamma^2}\frac{n_{\rm ld}}{n}\gamma_0'\frac{\beta_0'^2}{3} + \frac{\tilde{\Gamma}}{\Gamma}\left(1 + \gamma_0'\frac{n_{\rm ld}}{n}\right) = 1 + \gamma_0'\frac{n_{\rm ld}}{n}. \tag{63}$$

The form of this equation suggests that the rate of the flow deceleration due to pure mass loading does not depend on Γ, but on loading particle temperature, which is characterized by γ_0'. The result is shown in Fig. 4. For $n_{\rm ld}/n \ll 1$, the deceleration rate is given by

$$\frac{\dot{\Gamma}}{\Gamma} = -\frac{\dot{n}}{n}\gamma_0'\frac{\beta_0'^2}{3}. \tag{64}$$

Thus, the flow magnetization due to pure mass loading is defined by

$$\frac{\tilde{\sigma}}{\sigma} = \left[\frac{\tilde{\Gamma}}{\Gamma} + \frac{n_{\rm ld}}{n}\gamma_0'\left(\frac{\tilde{\Gamma}}{\Gamma} + \frac{\tilde{\Gamma}^2}{\Gamma^2}\frac{\beta_0'^2}{3}\right)\right]^{-1} \tag{65}$$

and it is always less than unity (see Fig. 5).

4.3 Acceleration along the jet due to field enhancement

If the c.m. velocity of a pair is much greater than the jet bulk velocity $\Gamma_0 \gg \Gamma$, we obtain the following expression for the average charge displacement using (56):

$$r_\perp = \frac{m_{\rm e}c^2}{e\tilde{B}}\frac{\Gamma_0\gamma_0'}{2}\left(1 + \frac{\beta_0'^2}{3}\right). \tag{66}$$

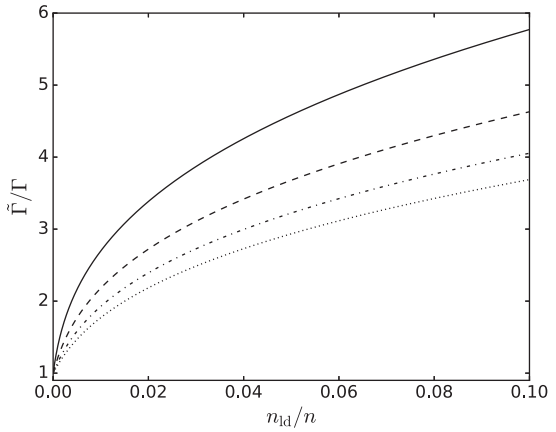

Figure 6. The plasma acceleration due to charge loading with pair c.m. having $\Gamma_0 = 10^3$. Ratio of the Lorentz factors after and before loading is plotted as a function of the relative loading particle number density $n_{\rm ld}/n$ for different Γ. The solid curve corresponds to $\Gamma = 5$, dashed to $\Gamma = 10$, dash–dotted to $\Gamma = 15$ and dotted to $\Gamma = 20$.

In this case, average charge separation is positive. This implies that instead of electric and magnetic field screening the enhancement of the fields takes place. The flow must accelerate due to such charge movement. This is easy to understand: opposite charges initially created in the same space point move in the opposite direction depending on the initial velocity of c.m. in the jet proper frame where the Lorentz force is due to B'. This induces a flow acceleration.

The Lorentz factor of a flow after loading, calculated as corresponding to the drift velocity in disturbed fields, satisfies the following algebraic equation:

$$-16\tilde{\Gamma}^6 + 16\tilde{\Gamma}^4 + \tilde{\Gamma}^3 16q\beta\Gamma^2 + \tilde{\Gamma}^2 16\Gamma^2\left(\Gamma^2 - 1\right) + \tilde{\Gamma}\left(-8q\beta\Gamma^2\right) + q^2 = 0, \tag{67}$$

where

$$q = \frac{4}{\sigma}\frac{n_{\rm ld}}{n}\Gamma_0\gamma_0'\left(1 + \frac{\beta_0'^2}{3}\right). \tag{68}$$

The appropriate solutions are presented in Fig. 6. As we see, the faster the flow, the slower it accelerates. For $n_{\rm ld}/n \ll 1$, the

acceleration rate is

$$\frac{\dot{\Gamma}}{\Gamma} = \frac{1}{\Gamma\sigma}\frac{\dot{n}}{n}\Gamma_0\gamma_0'\left(1+\frac{\beta_0'^2}{3}\right). \tag{69}$$

In order to compute the behaviour of a flow magnetization, we calculate the internal energy and anisotropic pressure through the corresponding energy-momentum tensor components. For $\Gamma_0 \gg \Gamma$, one can obtain

$$\begin{aligned} T_{\rm ld}^{00} &= m_{\rm e}c^2\Gamma n_{\rm ld}\left[\frac{1}{2}\Gamma_0\gamma_0'\left(1+\frac{\beta_0'^2}{3}\right)\left(1+\frac{\beta^2}{2}\right)\right. \\ &\left. +\ \Gamma^2\beta^2\frac{\gamma_0'}{\Gamma_0}\frac{\beta_0'^2}{3}\right], \\ T_{\rm ld}^{11} &= m_{\rm e}c^2\Gamma n_{\rm ld}\left[\frac{\gamma_0'}{\Gamma_0}\frac{\beta_0'^2}{3}+\frac{\Gamma_0\gamma_0'}{4\Gamma^2}\left(1+\frac{\beta_0'^2}{3}\right)\right], \end{aligned} \tag{70}$$

and

$$\begin{aligned} \varepsilon_{\rm ld} &= m_{\rm e}c^2 n_{\rm ld}\frac{\Gamma_0\gamma_0'}{2\Gamma}\left(1+\frac{\beta_0'^2}{3}\right), \\ P_{\rm s} &= T_{\rm ld}^{11}. \end{aligned} \tag{71}$$

Now using the magnetization definition (44) and obtained flow parameters (71), the following expression for the ratio of magnetizations after and before loading can be written as:

$$\frac{\tilde{\sigma}}{\sigma} = \frac{\tilde{S}K}{\tilde{K}S}, \tag{72}$$

where

$$\begin{aligned} \frac{\tilde{K}}{K} &= \frac{\tilde{\Gamma}}{\Gamma}+\frac{n_{\rm ld}}{n}\left[\frac{\Gamma_0\gamma_0'}{2\tilde{\Gamma}}\left(1+\frac{\beta_0'^2}{3}\right)\right. \\ &\left. +\ \frac{\tilde{\beta}}{\beta}\frac{\tilde{\Gamma}^3}{\Gamma^2}\left(\frac{\gamma_0'^2}{\Gamma_0}\frac{\beta_0'^2}{3}+\frac{\Gamma_0\gamma_0'}{4\tilde{\Gamma}^2}\left(1+\frac{\beta_0'^2}{3}\right)\right)\right], \end{aligned} \tag{73}$$

and the ratio $\tilde{S}/S$ can be readily computed using the following expression for the enhanced fields:

$$\tilde{B} = \frac{B}{2}\left[1+\sqrt{1+q\frac{\tilde{\Gamma}\tilde{\beta}}{\Gamma^2}}\right], \tag{74}$$

$$\tilde{E} = \frac{E}{2}\left[1+\sqrt{1+q\frac{\tilde{\Gamma}\tilde{\beta}}{\Gamma^2-1}}\right], \tag{75}$$

where q is defined by (68). As shown in Fig. 7, here again, although the plasma accelerates, the Poynting flux grows faster after loading than the plasma kinetic energy, so the magnetization is greater than unity.

Here we should stress that there are two different processes leading to a local plasma acceleration or deceleration. The first one is connected with the average charge separation, and the second one with the non-zero loading plasma temperature for the pure mass loading. In both cases, the average velocity of each of the created particles is equal to the fluid velocity. However, there is also a gyration motion that can be interpreted as the loading plasma temperature. This effective temperature is defined by the initial Lorentz factor in the pair c.m. system γ_0' and the corresponding velocity β_0'. The effects connected with the charge separation and the field screening cannot be erased by cooling of loaded plasma due to radiation or instabilities as $\beta_0' \to 0$. Indeed, once the pair is created, its average separation (25), (57) and (66) does not go to zero as $\beta_0' \to 0$. Thus, any process that wipes the gyration of loaded particles does not affect the field screening and, consequently, the appropriate plasma acceleration or deceleration. It is not so with the pure mass loading: the effect of a flow deceleration for a pure mass loading depends on the non-zero temperature [see (63) and (64)], so the bulk-plasma velocity does not change for $\beta_0' = 0$.

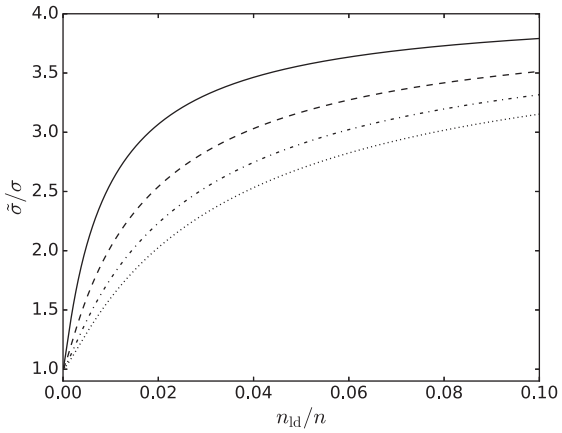

Figure 7. The plasma acceleration due to charge loading with pairs c.m. having $\Gamma_0 = 10^3$. Ratio of the flow magnetization after and before loading is plotted as a function of the relative loading particle number density $n_{\rm ld}/n$ for different Γ. The solid curve corresponds to $\Gamma = 5$, dashed to $\Gamma = 10$, dash–dotted to $\Gamma = 15$ and dotted to $\Gamma = 20$.

5 ASTROPHYSICAL APPLICATION

The process that can provide the appreciable number of pairs is a conversion of high-energy jet radiation with photon energies E_γ, propagating along the jet within opening angle $1/\Gamma$ in the laboratory frame, on the external soft photon field with photon energies $\epsilon_{\rm soft}$. The latter may be reprocessed by environment thermal radiation of an accretion disc, as suggested by Sikora, Begelman & Rees (1994). Such a process would account for the jet acceleration since the c.m. of these two photons have the Lorentz factor

$$\Gamma_0 = \sqrt{\frac{E_\gamma}{4\epsilon_{\rm soft}}}. \tag{76}$$

For soft photons in the infrared to ultraviolet range (10^{-2} to 10^2 eV) and reaction threshold condition, the Lorentz factor is in the 10^3–10^7 range along the jet. Thus, the pairs are created with c.m. moving faster than cold plasma before the charge loading, accelerating the jet plasma, as shown in Section 4.3. This process can operate naturally only on sub-parsec to parsec scales since there we may expect a strong enough soft photon field (Sikora et al. 1994).

The probability of a pair creation due to two-photon conversion has been studied in a number of works by Gould & Schreder (1967), Svensson (1982), Aharonian, Atoyan & Nagapetyan (1983) and Zdziarski (1988). The total pair creation rate due to reaction of γ-quanta with the number density N_γ on isotropically distributed soft photons with the number density $N_{\rm soft}$ is given by

$$\begin{aligned} \dot{n}_{\gamma\gamma} &= \frac{c}{2}\sigma_{\rm T}N_\gamma N_{\rm soft}\int_0^\infty {\rm d}x\,\tilde{n}_\gamma(x) \\ &\times\int_{1/x}^\infty {\rm d}y\,\tilde{n}_{\rm soft}(y)\frac{1}{x^2y^2}\varphi(xy), \end{aligned} \tag{77}$$

where $\tilde{n}_\gamma(x)$ is normalized to unity energy spectrum of γ-quanta depending on dimensionless energy $x = E_\gamma/m_{\rm e}c^2$ and $\tilde{n}_{\rm soft}(y)$ is the

same for soft photons with energy $\epsilon_{\rm soft} = ym_{\rm e}c^2$ (Svensson 1982). Here,

$$\varphi(xy) = \int_0^{xy} \frac{3}{8\pi r_0^2}\tilde{\sigma}_{\gamma\gamma}(s)s\,{\rm d}s \tag{78}$$

is averaged solid angle $\gamma\gamma \to e^+e^-$ reaction cross-section, $\sigma_{\rm T} = 8\pi r_0^2/3$ is a Thomson cross-section, $r_0 = e^2/m_{\rm e}c^2$ is a classical electron radius and $\sigma_{\rm T}\tilde{\sigma}_{\gamma\gamma}$ is a $\gamma\gamma \to e^+e^-$ cross-section (see e.g. Rybicki & Lightman 1979; Gould & Schreder 1967; Svensson 1982; Aharonian, Atoyan & Nagapetyan 1983; Zdziarski 1988). We use the asymptotic expression for $\varphi(xy)$, obtained by Gould & Schreder (1967). The reaction threshold condition is $xy \geq 1$.

The number density of soft photons may be estimated as

$$N_{\rm soft} = \frac{L_{\rm soft}}{4\pi R_{\rm soft}^2 c\langle\epsilon_{\rm soft}\rangle}, \tag{79}$$

and of γ-quanta as

$$N_\gamma = \frac{L_\gamma}{S_\gamma c\langle E_\gamma\rangle}. \tag{80}$$

Here, $L_{\rm soft}$ and L_γ are the corresponding luminosities. The first one is distributed isotropically over $4\pi R_{\rm soft}^2$, and for the second one we assume to be distributed over a jet cross-section in a laboratory frame. The $\langle E\rangle$ are averaged energy distribution of the corresponding photon fields.

Our aim is to obtain the luminosities, needed to account for the observed jet accelerations and deceleration. We take the monoenergetic photon spectra as the zero estimate. As $\varphi(xy)$ has a maximum of 0.21 (in the units of the Thomson cross section) at $xy \approx 3.5$ (Zdziarski 1988), we take a rough model for the high-energy conversion on soft photon field: $\epsilon_{\rm soft} = 1.6 \times 10^{-12}$ erg, $E_\gamma = 1.5$ erg. From these the pair c.m. Lorentz factor $\Gamma_0 = 4.8 \times 10^5$ and the initial charge energy in the c.m. frame $\gamma_0' = 1.8$ can be computed. This gives for the pair production rate

$$\dot{n}_{\gamma\gamma} = 8.8 \times 10^{-10}\Gamma^2\frac{L_{\rm soft,\,45}L_{\gamma,\,45}}{R^2_{\rm soft,\,pc}R^2_{\gamma,\,\rm pc}}\ {\rm cm^{-3}\,s^{-1}}. \tag{81}$$

Here, $(L/{\rm erg\,s^{-1}}) = 10^{45}L_{45}$.

As reported by Homan et al. (2015), the observed characteristic jet acceleration and deceleration rate is $\dot{\Gamma}/\Gamma \approx 10^{-3}$ to 10^{-2} yr^{-1} in a galaxy frame, or

$$\frac{\dot{\Gamma}}{\Gamma} = 3.1 \times 10^{-8} f\ {\rm s^{-1}}, \tag{82}$$

where f is 10^{-3} to 10^{-2} and is an observed factor of acceleration or deceleration. In order to account for such acceleration, we obtain from (69) the corresponding pair-creation rate as

$$\dot{n} = 2.9 \times 10^{-13} fn\ {\rm cm^{-3}s^{-1}}. \tag{83}$$

Thus, if we employ $n \approx 10^3$ cm^{-3} on a parsec distance (Lobanov 1998), $\Gamma \approx 10$ and $L_{\rm soft} \approx 10^{45}$ erg s^{-1} (Stern & Poutanen 2006), we need a luminosity of the order of 10^{40} erg s^{-1} in TeV radiation of a jet to explain the observed acceleration rate by the above-described process.

On the other hand, the deceleration may also occur due to conversion of two photons of high-energy jet radiation. For this reaction, the pairs are created with c.m. at rest in the jet proper frame on average since in the jet proper frame the radiation can be considered as isotropic. Thus, the results of Section 4.2 are applicable, and a jet deceleration due to pure mass loading takes place. This process can operate on scales greater than a few parsecs, where there is no substantial direct photon field from the disc or reprocessed by the clouds disc radiation. If we want to account for the observed deceleration rates on scales of a few 10 pc, the pair creation threshold condition implies that we need photons from the jet with energies greater than $E_\gamma = 1.5 \times 10^{-6}$ erg. From expression (81), rewritten for the photons of a jet radiation, we obtain the pair-production rate

$$\dot{n}_{\gamma\gamma} = 8.8 \times 10^{-12}L^2_{\gamma,\,45}\ {\rm cm^{-3}\,s^{-1}}. \tag{84}$$

Using (64) for the factor f, reported by Homan et al. (2015), we get $\dot{n}/n = 7.8 \times (10^{-12}{-}10^{-14})$ s^{-1}. Thus, to account for the observed deceleration rates, we need a luminosity in the laboratory frame $L \approx (3\text{–}9)10^{44}$ erg s^{-1} at MeV photons at a distance of 10 pc.

6 RESULTS AND DISCUSSION

The analysis of kinematic properties of bright features of relativistic jets (Homan et al. 2015) showed that the systematic accelerations and decelerations of bright features are normal among the jets. We propose a mechanism related to radiation that may change locally but significantly the bulk flow velocity, thus leading to the observed accelerations and decelerations.

The two-photon pair conversion process supplies a jet with charges of number density that can be estimated using the standard relations (77) and (78) (Gould & Schreder 1967; Svensson 1982; Zdziarski 1988), i.e. the process of mass and charge loading. We show that the latter is more important, since it leads to magnetic and electric field screening or enhancement, with the consequent influence on the flow motion in the domain of pair creation. We have shown that an important role in the process is connected with the motion of specific charges in the crossed electric and magnetic fields and with field screening or enhancement. The charge loading leads to a local change in such MHD outflow parameters as the angular velocity $\Omega_{\rm F}(\Psi)$ and the total current I. It is necessary to stress that such an initial charge separation is not wiped out with the end of gyromotion due to radiation or instabilities and thus the effect of field screening is unaffected by it.

The proposed mechanism works as a kind of radiation friction. Indeed, if the radiation field is such that the pair c.m. reference frame moves faster than the bulk flow, the charge gyration leads to the electric and magnetic field enhancement and the flow acceleration. For the pairs created due to hard γ-quanta of a jet radiation with the external soft isotropic radiation field, the c.m. Lorentz factor exceeds 10^3, which leads to extremely effective local flow acceleration even for loading pair number density as low as tenths of a per cent of the initial particle number density. Such pairs are mainly created close enough to the jet origin where the external radiation from the accretion disc provides a soft external radiation field (Sikora et al. 1994). For the pairs with the c.m. moving slower than the bulk flow velocity, local deceleration takes place either due to partial screening of electric and magnetic fields (see Section 3.2) or due to pure mass loading without significant field screening (see Section 4.2). The latter case is more probable as in the far jet domains there is no significant external radiation field, and pairs are mainly created due to interaction of internal jet photons, with the c.m. moving with the jet velocity on average.

Thus, the effect may account for the statistically significant accelerations of bright features of a jet at distances less than 50 pc and decelerations at further distances from the jet core as observed by MOJAVE programme.

The suggested mechanism of charge loading may play the role of a source of instabilities in a jet. The mirror instability (Rudakov & Sagdeev 1961) may wipe out the anisotropic pressure $P_{\rm s}$. However, discussed at the end of Section 4, this will not affect the process of

field screening and associated fluid local acceleration or deceleration. The mirror instability develops only for the weakly magnetized flows (Southwood & Kivelson 1993) – when the ratio of the plasma pressure to the magnetic pressure is greater than unity. Let us apply this criterion to the loaded flow considered in the previous sections. The anisotropic pressure P_s is exactly the T_{ld}^{11}, with the index '1' corresponding to the r-coordinate. Thus, it does not change with a transformation to the fluid frame. In the fluid frame, the ratio of the loaded plasma pressure to the magnetic pressure can be written as

$$\beta_m = \frac{P_s}{B'^2/8\pi}. \quad (85)$$

For the simplest case of a pair created at rest with respect to nucleus, the expression for P_s (23) gives

$$\beta_m = \frac{1}{\sigma}\frac{n_{ld}}{n}\Gamma, \quad (86)$$

with the outflow stability condition $\beta_m < 1$ being fulfilled for the flow satisfying the condition $\delta B/B < 1$ (29). For the pure mass loading (60),

$$\beta_m = \frac{2}{3}\frac{1}{\sigma}\frac{n_{ld}}{n}\gamma'_0\beta'^2_0, \quad (87)$$

and for pairs created with the c.m. moving faster than jet bulk velocity (70),

$$\beta_m = \frac{1}{\sigma}\frac{n_{ld}}{n}\left[\frac{2}{3}\frac{\Gamma\gamma'_0\beta'^2_0}{\Gamma_0} + \frac{\Gamma_0\gamma'_0}{2\Gamma}\left(1+\frac{\beta'^2_0}{3}\right)\right]. \quad (88)$$

Equations (86)–(88) provide the criteria of the mirror stability of the loaded flow; it is stable for $\beta_m < 1$.

As the average velocity of created chargesis equal to the fluid velocity, there is no current or beam of charged particles with respect to the flow in the pair creation region that can give rise to the Buneman (Buneman 1959; Iizuka et al. 1979) and two-stream instability. However, after the region of pair creation has been accelerated or decelerated, the above-presented picture of a sharp boundary of the uniform pair creation region may give rise to instabilities on the boundary loaded–non-loaded flow. In this case, the two-stream instability develops for the wave numbers $k < \omega_P/v_0$, where ω_P is a plasma frequency and v_0 is the velocity of loaded plasma with respect to non-loaded plasma. The preliminary estimates give

$$v_0 \approx \frac{c\Delta\Gamma}{\Gamma^3}. \quad (89)$$

Using the expression for $\Delta\Gamma$ (48) for the initial phase of the flow loading, we obtain

$$v_0 \approx c\frac{3}{\sigma\Gamma}\frac{n_{ld}}{n}. \quad (90)$$

So, unstable wavelengths are

$$\lambda > 3\frac{c}{\omega_P}\frac{n_{ld}}{n}\frac{1}{\sqrt{\sigma\Gamma}}. \quad (91)$$

The more realistic picture of gradual decrease of the loaded pair number density towards the jet axis due to external photon absorption may probably eliminate this possible source of such instabilities. However, this question deserves a separate analysis on the basis of the proposed mass-loading description.

These preliminary estimates show that the process of charge loading may lead to instabilities in the layer, where the mass and charge loading occurs. The question of the possible impact of instabilities on the proposed process will be addressed in the future work.

On the other hand, the same mechanism may account for the sights of radiation. Indeed, due to external Comptonized hard and external soft radiation and following pair creation, the local velocity of a bulk flow motion changes. This leads to possible appearance of internal shocks that in turn give rise to particle non-thermal acceleration, and following synchrotron radiation the external radiation thus working as a trigger for the internal radiation site.

ACKNOWLEDGEMENTS

We would like to thank M. Barkov, E. Derishev, Ya. N. Istomin and J. Poutanen for their useful comments. We also thank the unknown referee for the remarks regarding the stability question that helped to improve this paper. The study of mass and charge loading and its effects on the bulk plasma motion is supported by the Russian Fund for Basic Research (RFBR) grant 16-32-60074 mol_a_dk. The preliminary study of possible instabilities is supported by the Russian Science Foundation grant 16-12-10051.

REFERENCES

Aharonian F. A., Atoyan A. M., Nagapetyan A. M., 1983, Astrophysics, 19, 187
Asséo E., Beaufils D., 1983, Ap&SS, 89, 133
Beskin V. S., 2009, MHD Flows in Compact Astrophysical Objects. Springer-Verlag, Berlin
Beskin V. S., 2010, Phys.-Usp., 53, 1199
Beskin V. S., Chernoglazov A. V., 2016, MNRAS, 483, 3398
Buneman O., 1959, Phys. Rev., 115, 503
Derishev E. V., Aharonian F. A., Kocharovsky V. V., Kocharovsky Vl.V., 2003, Phys. Rev. D, 68, 043003
Ferraro V. C. A., 1937, MNRAS, 97, 458
Gould R. J., Schréder G. P., 1967, Phys. Rev., 155, 1404
Homan D. C., Lister M. L., Kovalev Y. Y., Pushkarev A. B., Savolainen T., Kellermann K. I., Richards J. L., Ros E., 2015, ApJ, 798, 16
Iizuka S., Saeki K., Sato N., Hatta Y., 1979, Phys. Rev. Letters, 43, 1404
Kuznetsova I. V., 2005, ApJ, 618, 432
Lichnerowicz A., 1967, Relativistic Hydrodynamics and Magnetodynamics. Benjamin, New York
Lobanov A. P., 1998, A&A, 330, 79
Lyutikov M., 2003, MNRAS, 339, 623
Rudakov L. I., Sagdeev R. Z., 1961, Dokl. Acad. Nauk SSSR, 6, 415
Rybicki G. B., Lightman A. P., 1979, Radiative Process in Astrophysics. Wiley-VCH, New York
Sikora M., Begelman M.C, Rees M. J., 1994, ApJ, 421, 153
Southwood D. J., Kivelson M. G., 1993, J. Geophys. Res., 98, 9181
Stern B. E., Poutanen J., 2006, MNRAS, 372, 1217
Stern B. E., Poutanen J., 2008, MNRAS, 383, 1695
Svensson R., 1982, ApJ, 258, 335
Tchekhovskoy A., McKinney J., Narayan R., 2009, ApJ, 699, 1789
Tsikarishvili E. G., Rogava A. D., Tsikauri D. G., 1995, ApJ, 439, 822
Zdziarski A. A., 1988, ApJ, 335, 786

APPENDIX A: AVERAGING PROCEDURE

To average a τ-dependent function $A(\tau)$ with respect to laboratory time one has to use the following relation:

$$\langle A\rangle = \frac{1}{T}\int_0^T A(\tau)\mathrm{d}t = \frac{1}{\int_0^{T'}\gamma(\tau)\mathrm{d}\tau}\int_0^{T'} A(\tau)\gamma(\tau)\mathrm{d}\tau. \quad (A1)$$

Here T' is an appropriate period in the loading particle rest frame.

The averaging procedure for components of the energy-momentum tensor T^{ik} is as follows. $T_{ld}^{ik} = mc^2\langle n_{ld}^{rest}u^i u^k\rangle$ contains the thermodynamical parameters in the particle rest frame. For instance, the appropriate particle number density n_{ld}^{rest} is related to the particle number density n_{ld}^{lab} in the laboratory frame by $n_{ld}^{lab} = \gamma(\tau)n_{ld}^{rest}$. The components T_{ld}^{ik} after the averaging procedure

have to be written using the thermodynamical parameters in the jet reference frame, i.e. $n_{\rm ld}$ – particle number density in the jet frame. As $n_{\rm ld}^{\rm lab} = \Gamma n_{\rm ld}$, we write the energy-momentum tensor components as

$$T_{\rm ld}^{ik} = mc^2 \langle n_{\rm ld}^{\rm rest} u^i u^k \rangle = mc^2 \Gamma n_{\rm ld} \left\langle \frac{u^i u^k}{\gamma(\tau)} \right\rangle . \tag{A2}$$

Finally,

$$T_{\rm ld}^{ik} = mc^2 \Gamma n_{\rm ld} \frac{1}{\int_0^{T'} \gamma(\tau) {\rm d}\tau} \int_0^{T'} u^i(\tau) u^k(\tau) {\rm d}\tau . \tag{A3}$$

APPENDIX B: ENERGY-MOMENTUM TENSOR FOR LOADED PARTICLES

The non-zero components of the energy-momentum tensor $T_{\rm ld}^{ik} = \langle mc^2 n_{\rm ld}^{\rm rest} u^i u^k \rangle$ in the laboratory reference frame obtained by the averaging procedure are the following:

$$T_{\rm ld}^{00} = mc^2 \Gamma^3 n_{\rm ld} \left(1 + \frac{\beta^4}{2} \right) , \tag{B1}$$

$$T_{\rm ld}^{02} = mc^2 \Gamma^3 n_{\rm ld} \beta \sin\alpha \left(1 + \frac{\beta^2}{2} \right) , \tag{B2}$$

$$T_{\rm ld}^{03} = mc^2 \Gamma^3 n_{\rm ld} \beta \cos\alpha \left(1 + \frac{\beta^2}{2} \right) , \tag{B3}$$

$$T_{\rm ld}^{11} = mc^2 \Gamma n_{\rm ld} \frac{\beta^2}{2} , \tag{B4}$$

$$T_{\rm ld}^{22} = mc^2 \Gamma^3 n_{\rm ld} \sin^2\alpha \frac{3\beta^2}{2} , \tag{B5}$$

$$T_{\rm ld}^{23} = mc^2 \Gamma^3 n_{\rm ld} \sin\alpha \cos\alpha \frac{3\beta^2}{2} , \tag{B6}$$

$$T_{\rm ld}^{33} = mc^2 \Gamma^3 n_{\rm ld} \cos^2\alpha \frac{3\beta^2}{2} . \tag{B7}$$

The components of hydrodynamical four-velocities in the laboratory frame are

$$U^0 = \Gamma , \tag{B8}$$

$$U^1 = 0 , \tag{B9}$$

$$U^2 = \beta\Gamma \sin\alpha , \tag{B10}$$

$$U^3 = \beta\Gamma \cos\alpha . \tag{B11}$$

Lichnerowicz vector components are

$$b^i = \left\{ 0;\ 0;\ -\frac{B}{\Gamma} \sin\alpha ;\ \frac{B}{\Gamma} \cos\alpha \right\} . \tag{B12}$$

APPENDIX C: ALGEBRAIC EQUATION ON THE SELF-CONSISTENT LORENTZ FACTOR OF THE CHARGE LOADED OUTFLOW

When the screening/enhancement of the fields takes place, it is convenient to find the general algebraic equation for $\tilde{\Gamma}$. Let us introduce the dimensionless factor F:

$$r_\perp = \frac{m_{\rm e} c^2}{e\tilde{B}} F . \tag{C1}$$

The exact expression for the self-similar charge loaded flow velocity is

$$\tilde{\beta} = \beta \frac{1 + \sqrt{1 + Q/(\Gamma^2 - 1)}}{1 + \sqrt{1 + Q/\Gamma^2}} . \tag{C2}$$

In a physically interesting case of $Q/\Gamma^2 \ll 1$, the general algebraic equation on $\tilde{\Gamma}$ for the given $r_\perp(F)$ is the following:

$$Q^3 \tilde{\Gamma}^2 \frac{\Gamma^6 + 7\Gamma^4 - 10\Gamma^2 + 4}{32\Gamma^4 \left(\Gamma^2 - 1\right)^3} + Q^2 \tilde{\Gamma}^2 \frac{-3\Gamma^2 + 2}{8\Gamma^2 \left(\Gamma^2 - 1\right)^2} + Q\tilde{\Gamma}^2 \frac{1}{2\left(\Gamma^2 - 1\right)} - \tilde{\Gamma}^2 + \Gamma^2 = 0 , \tag{C3}$$

where parameter

$$Q = \frac{4}{\sigma} \frac{n_{\rm ld}}{n} \tilde{\Gamma} F . \tag{C4}$$

This is a third-order decomposition over Q/Γ^2 which reproduces, with high accuracy, the exact equation (33) for the special case of pairs created at rest in a nucleus rest frame.

This paper has been typeset from a TEX/LATEX file prepared by the author.